Desalination and Water Treatment
www.deswater.com
doi: 10.5004/dwt.2022.29107

279 (2022) 187–194
December

Hydrodynamics modeling and electrochemical performance of a lab-scale single-channel cell through residence time distribution and kinetic studies

Taha Zier[a,*], Souad Bouafia[a], Youcef Rechidi[b], Malika Chabani[a]

[a]*Laboratoire Génie de la Réaction, Faculté de Génie des Procédés et Génie Mécanique, USTHB, BP 32, El Allia, Bab Ezzouar, Algérie, email: tzier@usthb.dz (T. Zier)*
[b]*Laboratoire d'analyse et de contrôle de la raffinerie d'Alger, SONATRACH, Sidi Arcine, Baraki, Algérie*

Received 30 June 2022; Accepted 27 September 2022

ABSTRACT

The present work investigated the electrochemical performance of a 3D-printed lab-scale electrochemical cell frame doped with turbulent cylindrical promoters at the inlet using as a case study the treatment of Algiers refinery effluent. Residence time distribution (RTD) experiments were conducted to characterize the flow developed in the reaction environment. A kinetic study of chemical oxygen demand removal of the effluent was aimed to access the reaction rates. Results indicated that the experimental data from RTD fitted well the axially dispersed plug flow (AD-PFR) model with semi-infinite boundary conditions, whereas the kinetic response showed an agreement with a pseudo-first-order model. The mean residence time, the Peclet number (Pe) and the axial dispersion were estimated at 2.07s, 8.36 and 0.0012 m^2/s, respectively. Interestingly, the results revealed a high dispersion for relatively low Reynolds number (Re) in the channel. This reflected the applicability of the proposed inlet design to treat low-loaded feeds at higher currents. Finally, the species residence time and the drag forces interaction on the electrode passivation was discussed and future implementation of the proposed inlet design was emphasized.

Keywords: Electro-oxidation; Axial dispersion model; Static-mixing; Cell design; Petroleum refinery effluent

1. Introduction

At the heart of the global dilemma, the petroleum processing industry, which is among the largest users of water resources, accounts for up to a third of the world's energy usage [1]. Fresh water quality and availability is affected due to the discharges large volumes of wastewater. The presence of a variety of recalcitrant pollutants, has made it difficult for effective treatment of petroleum refinery effluents [2].

The need for non-conventional sources of clean water and sustainable energy has pushed research boundaries worldwide to find reliable and efficient technologies for waste water treatment and reuse [3]. Electrochemical processes are regarded as green and versatile technologies [4,5]. The long-term goal for this technology is to go from lab to large-scale applications. However, currently the main drawbacks are oxidation by-products, energy consumption and low space-time yield.

Unlike empirical investigations, theoretical modeling can provide a reliable description of the electrochemical oxidation process. The later can offer a better account of the competition between desired reactive paths and side reactions, as well as deeper understanding of the transfer phenomenon and flow patterns in the reaction environment [6]. Moreover, the experimental validation of mathematical models can confirm modeling assumptions, providing precious data for further research comparisons and concrete insights towards up-scaling. Several authors have reported investigations of electrochemical cells for organic compounds remediation employing kinetic [7–10] and

* Corresponding author.

Presented at the First International Congress of Energy and Industrial Process Engineering (ICEIPE'22) 23–25 May 2022, Algiers, Algeria

hydrodynamic models [11–13]. Recent trends were towards computational fluid dynamics (CFD) studies combined with residence time distribution (RTD) and pressure-drop experiments as powerful tools in the design and characterization of electrochemical reactors [14,15].

Despite advances in electro-oxidation technology in the wastewater treatment industry, there is still a need for a more systematic approach in the scaling up process [16]. Electrochemical advanced oxidation processes (EAOPs) can be implemented at the pre-treatment or polishing stage given their versatility, to combust or convert the pollutants into more biodegradable forms [16–18]. Although process performance is function of several parameters, namely anode material, effluent nature and concentration, pH, hydrodynamics and current density [19], the technical feasibility is primarily judged by energy efficiency. System inefficiencies technically are due to mass polarization, activation over-potential and ohmic resistance.

From a process engineering perspective, the current study addressed electrode poisoning over-potential constraint in the direct electro-oxidation process through cell design and hydrodynamic characterization. The reactions of interest required the direct contact of the pollutants with the electrode surface. Therefore the mass transfer from and towards the catalytic surface of the anode was the bottleneck of the technology [20]. Hence, a proper hydrodynamic regime is crucial.

In this paper, the cell inlet design and hydrodynamics effect on the electrochemical performance were investigated to assess catalytic surface poisoning over-potential and thus the over-all process efficiency. The flow characterization and reaction rates as function of flow velocity and current density, in respect to the anodic oxidation of an Algiers refinery effluent, were examined and discussed.

2. Theory and hypothesis

2.1. Operating regime and kinetic model

The general mechanism for electrochemical oxidation of organics in wastewater assumes that the initial reaction is water discharge at potentials over 1.23 V/SHE [21], leading to the formation of a physisorbed hydroxyl radical at the anode surface [Eq. (1)].

$$\mathrm{M} + \mathrm{H_2O} \rightarrow \mathrm{M(OH)} + \mathrm{H} + \mathrm{e^-} \tag{1}$$

The electrochemical and chemical reactivity of the electro-generated hydroxyl radical depended on the anode material, hence the rate of reaction in competition [22]. Active anodes are characterized by a strongly adsorbed hydroxyl radical, which is suspected to form a higher oxide according to reaction [Eq. (1)]. The higher oxide acted as a selective mediator in organics oxidation, which compete with the oxygen evolution reaction (OER) [Eqs. (2)–(4)].

$$\mathrm{M(OH)} \rightarrow \mathrm{MO} + \mathrm{H} + \mathrm{e^-} \tag{2}$$

$$\mathrm{MO} + \mathrm{RH} \rightarrow \mathrm{M} + \mathrm{RO} \tag{3}$$

$$\mathrm{MO} \rightarrow M + \frac{1}{2}\mathrm{O_2} \tag{4}$$

Whereas non-active anodes presented a weak interaction between the hydroxyl radical and the anode surface, allowing the direct reaction with organics to yield complete mineralization [Eq. (5)].

$$\mathrm{RH_{aq}} + a\mathrm{M(OH)_{ads}} \rightarrow \mathrm{M} + m\mathrm{CO_2} + n\mathrm{H_2O} + x\mathrm{H} + y\mathrm{e^-} \tag{5}$$

This reaction was also in competition with OER and dimerization to hydrogen peroxide [Eqs. (6) and (7)].

$$\mathrm{M(OH)_{ads}} \rightarrow \mathrm{M} + \frac{1}{2}\mathrm{O_2} + \mathrm{H} + \mathrm{e^-} \tag{6}$$

$$2\mathrm{M(OH)} \rightarrow 2\mathrm{M} + \mathrm{H_2O_2} \tag{7}$$

In this case study, the cell was equipped with graphite, which was reported as modified active anode [23]. Therefore, the effluent biodegradability was expected to be enhanced remarkably compared to pollutants removal. For the sake of simplicity, the following assumptions were considered:

- OER was the only competitive reaction;
- The process was mass transfer controlled;
- Current density was uniformly distributed in the cell;
- Oxidation of organics took place only at the anode (i.e., nonhomogeneous oxidation in the bulk).

Assuming mass transport regime implied operating under relatively high current densities (i.e., abundance of hydroxyl radicals) and low-loaded feed. Subsequently, the kinetics were simplified to a pseudo-first-order reaction, hence [Eq. (8)]:

$$r = -\frac{\partial C_0}{\partial t} = k_{\mathrm{app}} C \tag{8}$$

Several models were proposed through the literature to describe electro-oxidation kinetics of organics abatement. Comninellis et al. [21] developed a theoretical relation between current efficiency and operating parameters, where the process performance was predicted once the mass transfer coefficient was estimated through a simple current-limiting experiment [24] [Eq. (9)].

$$C_t = C_0 \exp\left[-\left(\frac{Ak_m}{V_r}\right)t\right] \tag{9}$$

The mass transfer coefficient was reciprocally computed given access to experimental concentration measurements through fitting the experimental data to Eq. (9).

2.2. Geometry and flow model

The treatment process required adequate contact between the organic substrate and the catalyst surface. Consequently, the need for significance of flow characterization [25,26]. It was assumed that a plug flow model represented the system, considering dispersion processes within the cell, and supposing an ideal pulse injection at the inlet, the degree of dispersion was investigated by fitting the experimental RTD data with the axial dispersion model (ADM). The concentration of the species was given by Eq. (10):

$$\frac{\partial c}{\partial t} = D_{\text{eff}} \frac{\partial^2 c}{\partial x^2} - u \frac{\partial c}{\partial x} \tag{10}$$

Which may be rewritten in its dimensionless form as Eq. (11);

$$\frac{\partial C}{\partial \theta} = \frac{1}{\text{Pe}} \frac{\partial^2 C}{\partial x^2} - u \frac{\partial C}{\partial x} \tag{11}$$

where C was the dimensionless tracer concentration, Pe the Peclet number describing flow dispersion, θ dimensionless time and x the axial length. The dimensionless parameters were ([Eq. (12)] (nomenclature):

$$C = \frac{c}{c_0}; \theta = \frac{t}{\bar{t}_s}; \text{Pe} = \nu \frac{l_d}{D_0} \xi \tag{12}$$

where c was the tracer concentration at the outlet, c_0 the initial tracer concentration, x the axis coordinate along the cell diagonal, l_d the diagonal length, t the time, $\bar{t}_S$ the mean residence time, v the average liquid velocity in the empty channel, ξ the void fraction (ξ = 1 in empty channels) and D_0 the dispersion coefficient.

The geometry consisted of a channel with cylindrical deflectors at the extremes (Fig. 1). Consequently, ideal plug-flow was assumed before the cell inlet together with the same degree of dispersion inside and after the cell outlet. Hence, the appropriate boundary condition should have been "Semi-infinite" boundary condition [11]. The initial condition was therefore given by Eq. (13):

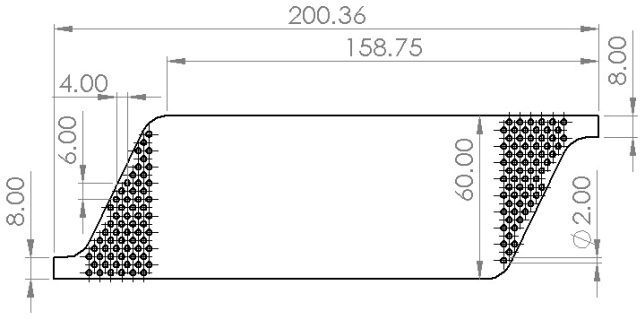

Fig. 1. Drawing and the dimensions of the electrochemical cell in mm.

$$C_{(0,t)} = \frac{c_0 Q}{\left(V / l_d\right)\nu} \delta t \tag{13}$$

The resulting expression for the normalized concentration was [Eq. (14)]:

$$E'(\theta) = \sqrt{\frac{\text{Pe}}{4\pi\theta^3}} \exp\left(\frac{-\text{Pe}(1-\theta)^2}{4\theta}\right) \tag{14}$$

Pe was first estimated by the moment method [Eq. (15)], and eventually computed through Eq. (14).

$$\frac{\sigma^2}{\bar{t}_s^2} = \frac{2}{\text{Pe}} - \frac{2}{\text{Pe}^2}\left(1 - \exp(-\text{Pe})\right) \tag{15}$$

3. Materials and methods

3.1. Experimental set-up

The experimental study was performed on a 3D-printed mono-channel electrochemical cell doped with turbulent cylindrical promoters as shown in Fig. 1. The cell was designed and printed with 1.75 PLA filament using a 3D-printer (Anycubic i3 Mega). Table 1 summarizes the main printing parameters to ensure a watertight frame.

Fig. 2 illustrates the flow circuit. The solution flowed through a plastic pipe with a diameter of 8 mm. The centrifuge pump propelled the solution from the storage tank to the electrochemical cell, through the pipe, and back to the storage tank. More details about the set-up specifications are addressed in Table 2.

3.2. Residence time distribution

Initially, water was run through the cell at specific flow rates until the flow was judged stable. Then the residence time distribution (RTD) experiments were performed. This was based on tracer pulse injection where

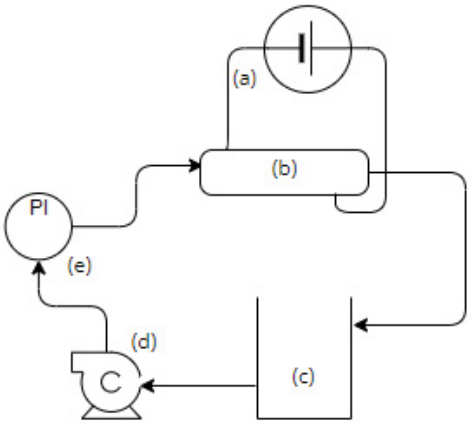

Fig. 2. Schematic diagram of the flow circuit. (a) DC power supply, (b) electrochemical cell, (c) mixed tank, (d) centrifugal pump and (e) pressure indicator.

a shot of concentrated salt (1 mL of 5M calcium chloride) was injected into the inlet. The injection took a fraction of a second and was therefore considered instantaneous. The concentration of the tracer at the outlet of the cell was monitored as a function of time. Concentrations were determined by measuring the conductivity variation at different flow rates. The normalized concentration $E(t)$ was calculated using Eqs. (16) and (17). Subsequently, the Peclet number (Pe) was obtained by the analytical solution of Eq. (14), which determined the $E'(\theta)$ value in dimensionless times. Specifically, the Pe number in Eq. (14) was computed through the non-linear least-square method using an Excel sheet to best fit $E'(\theta)$ with respect to the experimental curve $E(\theta)$.

$$E(t) = \frac{C}{\int_0^t C dt} \tag{16}$$

$$\bar{t}_s = \int_0^t tE(t) \tag{17}$$

Subsequently, the axial dispersion coefficient (D_0) was computed through Eq. (18):

$$D_0 = \frac{\nu l_d}{\mathrm{Pe}} \tag{18}$$

where v and l are the mean channel velocity and the channel diagonal, respectively. Finally, the Reynolds number (Re) was calculated using Eqs. (19) and (20):

$$\mathrm{Re} = \frac{d_e \nu}{\vartheta} \tag{19}$$

Table 1
Main printing parameters

Layer high (mm)	0.06
Wall thickness (mm)	1.6
Infill density (%)	100
Printing temperature (°C)	210
Build plate temperature (°C)	70
Minimum support X/Y distance (mm)	0.4

Table 2
Set-up specifications

Cell volume (mL)	110
Storage tank volume (mL)	750
Total volume (mL)	1,000
Inter-electrode gap (mm)	12
Anode/cathode plate dimensions (mm)	140 × 80
Active area (cm^2)	78
Surface/reactor volume ratio	7.8
Reactor volume/total volume ratio	0.11

$$d_e = \frac{2 d_C w_C}{\left(d_C + w_C\right)} \tag{20}$$

where ϑ is the kinematic viscosity, and d_e is the hydraulic diameter of the channel, which is defined by the inter-electrode gap d_c and the width of the cell w_c.

3.3. Electro-oxidation of organic compounds

The electrochemical cell was designed to enhance the biodegradability of refinery effluent at the lab-scale. Therefore, a combination of graphite anode and a stainless-steal cathode was employed. The real effluent samples were taken at the dissolved air flotation (DAF) outlet at the Algiers case study site, before the biological treatment. The effluent characteristics were not the same at various times. The average values are reported in Table 3. Each experiment was run for 60 min and used 1 L of effluent. The main variable operating parameter is reported in Table 4. Before treatment, 0.1 M of sodium sulfate was added to reduce the ohmic over-potential. The cell was powered by a direct current supply (AD-305D, AIDA, China), and operated in galvanostatic mode.

3.4. Analytical procedures

All solutions were prepared with distillated water and all experiments were performed at room temperature (i.e., at 20°C ± 2°C). To determine the chemical oxygen demand (COD), samples were transferred to a spectrophotometer (Jenway 6305 UV/Vis, United Kingdom) at 600 nm, following the standard method (MA315-DCO-1.1). Electrical energy specific consumption (EESC) and current efficiency (CE) were computed as follows [Eqs. (21) and (22)]:

$$\mathrm{EESC}\left(\mathrm{KWh.kg^{-1}}\right) = \frac{UIt}{\Delta \mathrm{COD} V_r} \tag{21}$$

Table 3
Characteristics of real effluent

Temperature (°C)	20
MES (mg/L)	143
Conductivity (mS)	2.44
pH	9.11
COD (mg/L)	500–600
Phenols (mg/L)	10.7

Table 4
Investigated flow rate range and relevant data

Flow rate (mL/min)	Transit time (s)	Pressure drop (Pa)	$\mathrm{Re}_{\mathrm{inlet}}$	$\mathrm{Re}_{\mathrm{channel}}$
1,304	5.06	5,000	3,460	603
1,430	4.61	6,895	3,795	662
1,580	4.18	10,000	4,193	731
1,667	3.96	10,342	4,424	771
2,100	3.14	13,790	5,573	972

$$\mathrm{CE}(\%) = \frac{\mathrm{FV}_r \Delta\mathrm{COD}}{8It} \tag{22}$$

4. Results and discussion

4.1. Pressure-drop

Experimental results showed that the pressure drop obeyed a logarithmic function of flow velocity, expressed in term of Re. Fig. 3 illustrates agreement (R^2 = 0.94) between experimental and fitted data. The experimental data was correlated with the Reynolds number in the channel through Eq. (23).

$$\Delta p = a\,\mathrm{Re}^b \tag{23}$$

where a and b were 2×10^{-2} and 1.97, respectively. The value of the constant "a" was smaller than those reported in the literature [27], which was balanced by a high value of "b". Similar trends were reported elsewhere [28].

4.2. Residence time distribution

Table 4 summarizes the experimental flow rate range and relevant flow parameters. RTD response was examined using experimental $E(\theta)$ and calculated $E'(\theta)$ curves as function of the flow conditions where the function $E'(\theta)$ quantified the degree of axial dispersion into the cell. Fig. 4 shows that the axial dispersion model (ADM) described correctly the RTD curve at Re numbers higher than 972 (2,100 mL/min). The experimental results showed a slight increase in Peclet number with the flow velocity, which reflected the tendency towards plug flow, and therefore better performance of the cell at high flow rates. However, at lower Re (<972), the liquid flow pattern deviated considerably from the ADM which reflects the presence of stagnant zones. Accordingly, plug dispersion exchange (PDE) model was more appropriate to describe the mass transfer of species between stagnant and dynamic zones. The back-mixing phenomenon encountered at lower Re was mitigated through adequate implementation of deflectors, which enhanced substantially macro-mixing and promoted turbulence. Several studies reported on the major contribution of cell geometry and turbulent promoters in electrochemical cells [28–30], where their unique design and engraving was the proper added value of the cell [31].

Straightforward RTD curve analysis was through the first and the second moments, accounting for the physical mean residence time of species in the reactor and its variance, respectively. The mean residence time, the Peclet number and the axial dispersion were estimated at operating flow rate of 2,100 mL/min by 2.07 s [Eq. (17)], 8.63 and 0.0012 m²/s [Eq. (12)], respectively. Compared to the well-known FM01-LC cell with PTFE turbulent promoter, the proposed frame presented the same Peclet number at roughly half the flow mean velocity developed between the electrodes [11]. Although more insights regarding pressure drop are necessary for proper comparison, the axial dispersion developed at a similar velocity reflected the cylindrical shape efficiency in promoting homogeneous velocity profiles throughout the channel at lower operating costs.

The RTD analysis suggested that the suitable operating regimes were at inlet Reynolds numbers above 5,573, where the dead-volumes and by-pass phenomenon were minimized and a plug-flow trend was developed at the reaction environment. Hence, the choice of the flow rate for kinetic study of organics removals.

4.3. Kinetic study

The kinetics of COD removal were investigated at the extremes of the flow rate range. The experimental results obtained in galvanostatic electrolysis and those predicated by the pseudo-first-order model are presented in Figs. 5 and 6, at flow rates of 1,304 and 2,100 mL/min, respectively. Good agreement was achieved (R^2 = 0.99). The reaction rates (k_{app}) were estimated through linear regression, subsequently the mass transfer coefficient was computed [Eq. (9)]. Table 5 summarizes the main results.

As shown in Fig. 5, the reaction rate increased with the current density accounting for roughly a double increase in energy consumption and a lower current efficiency (Table 5). This behavior reflected the process operating at mass transfer control, at which side reactions (mainly oxygen evolution) occurred with applied current [32]. Poor mass transfer hindered the efficient depletion of hydroxyl radicals as the

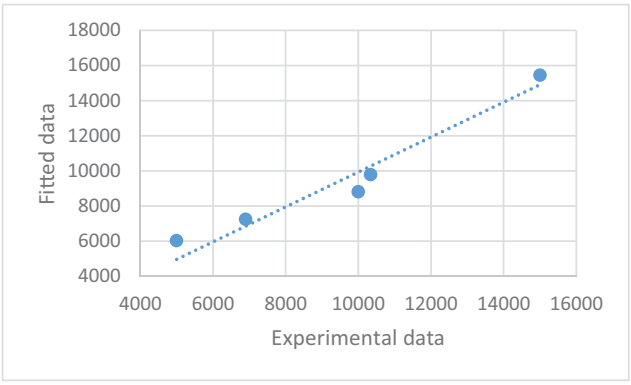

Fig. 3. Experimental vs. theoretical pressure-drop data.

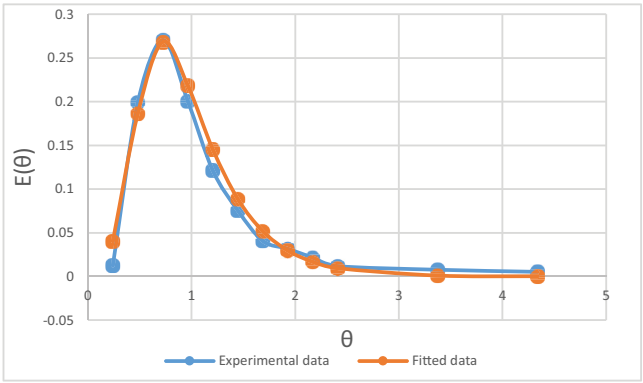

Fig. 4. Experimental vs. theoretical RTD curves at flow rate of 2,100 mL/min.

Table 5
Main responses reported from the effluent electro-oxidation

Flow rate (mL/min)	Current density (mA/cm^2)	EESC (kWh/kg)	CE (%)	k_{app} (min^{-1})	k_m (cm/s)
1,304	12.8	47.62	49	0.0053	0.068
	20.5	80	34	0.0064	0.082
2,100	20.5	55.14	37	0.0084	0.108

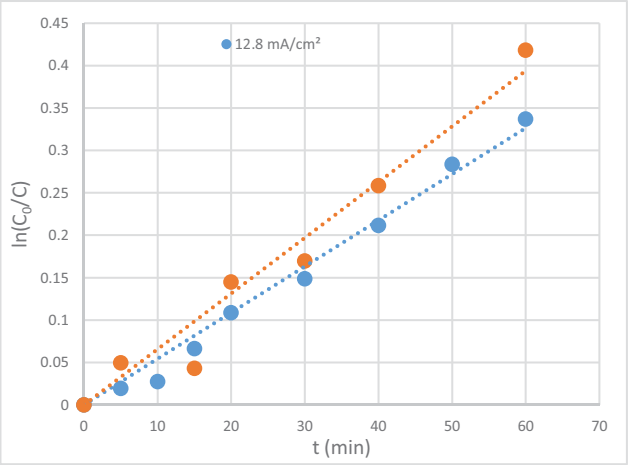

Fig. 5. COD abatement at flow rate of 1,304 mL/min.

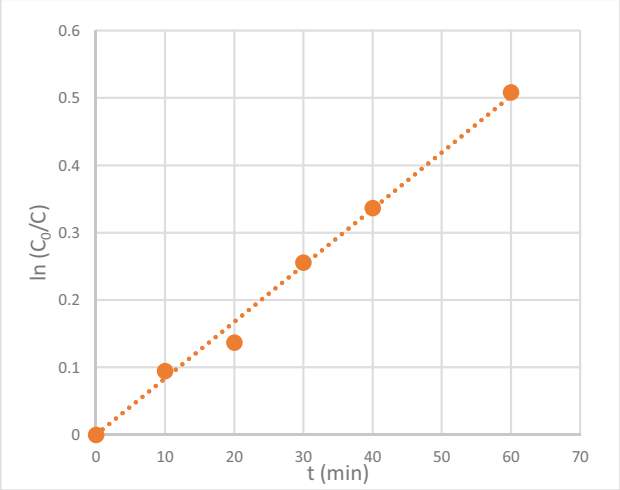

Fig. 6. COD abatement at 2,100 mL/min and 20.5 mA/cm^2.

desired reactions required the direct contact between organic substrates and the catalytic surface. As indeed, higher hydroxyl radical production rates increased the probability of collusion with pollutants, which implied a respectable removal rate observed as a slight increase in the estimated mass transfer coefficient. However, this was at the cost of process efficiency. Thus, current density had a negative effect on pollutants removal. Similar trends were reported elsewhere [33].

In the other hand, Fig. 6 demonstrates the effect of operating flow rate, at a high value of applied current density. The reaction rate rose substantially with the flow velocity. Moreover, a drastic decrease in energy consumption was observed alongside mass transfer coefficient enhancement and a rise in current efficiency (Table 5). This behavior was explained by organic substrates present at the anode in comparison to the active sites at the surface. Furthermore, the applied shear stress allowed for better exchange of mass, both through sweeping the reaction products and shrinking the diffusion boundary layer. Electrode poisoning over-potential, referring to the mass transport polarization, alongside activation over-potential and ohmic resistance, accounted for electrochemical cell inefficiency [25]. Operating under proper hydrodynamic condition, residence time and drag forces were optimized.

Under the given flow rate and desired feed load, the optimum current could be estimated through a simple limiting-current technique [34]. However, going for a three-electrode configuration in compact cells was a complicated task. Selecting the flow rate based on flow characterization suggested operating at current densities below 20 mA/cm^2, as the path of operating at higher currents for productivity came with the costs of loses in process selectivity and energy consumption.

5. Concluding remarks

Results indicated that at operating flow rate of 2,100 mL/min ($Re_{channel}$ = 972) the flow obeyed the axial dispersion model (ADM). Organic substrate decay followed a pseudo-first-order reaction. The reaction rates were found to increase with applied current, whereas sever loses in process selectivity and energy consumption were encountered. This trend supported the mass transport-controlled regime hypotheses. Moreover, the cell inlet design was found to substantially promote turbulence at low fluid velocities compared to other mesh configurations found in the literature. Thus, giving rise to its potential applicability in treating further low-loaded feeds at higher currents.

To conclude, the study demonstrated the crucial role of cell design through theoretical modeling in process up-scaling. There is a need to further investigate the interaction of the applied shear stress by the electrolyte and species residence time on the catalytic surface passivation.

Acknowledgment

Authors would like to acknowledge the support of DGRSDT, Snai3i and SONATRACH.

Symbols

A	—	Electrode active area
C	—	Dimensionless concentration
c	—	Concentration
d_c	—	Inter-electrode gap
d_e	—	Hydraulic diameter of the channel
D_0	—	Axial dispersion coefficient
D_{eff}	—	Effective diffusion
E(t)	—	Normalized experimental concentration
E'(t)	—	Normalized theoretical concentration
F	—	Faraday constant
I	—	Applied current
k_{app}	—	Reaction constant
k_m	—	Mass transfer coefficient
l	—	Length of the cell
p	—	Pressure
Pe	—	Peclet number
Q	—	Volumetric flow rate
Re	—	Reynolds number
r	—	Reaction rate
$\bar{t}_S$	—	Mean residence time
v	—	Averaged flow velocity
ϑ	—	Kinematic viscosity
V	—	Geometric volume of the cell
V_r	—	Reactor volume
u	—	Instantaneous flow velocity
U	—	Applied voltage
w_c	—	Width of the cell

Greek

θ	—	Dimensionless time
σ^2	—	Residence time variance
ξ	—	Void fraction

References

[1] M. Bartolomeu, M.G.P.M.S. Neves, M.A.F. Faustino, A. Almeida, Wastewater chemical contaminants: remediation by advanced oxidation processes, Photochem. Photobiol. Sci., 17 (2018) 1573–1598.

[2] B.H. Diya'Uddeen, W.M.A.W. Daud, A.R. Abdul Aziz, Treatment technologies for petroleum refinery effluents: a review, Process Saf. Environ. Prot., 9 (2011) 95–105.

[3] J. de J. Treviño-Reséndez, A. Medel, Y. Meas, Electrochemical technologies for treating petroleum industry wastewater, Curr. Opin. Electrochem., 27 (2021) 100690, doi: 10.1016/j.coelec.2021.100690.

[4] S. Garcia-Segura, J.D. Ocon, M.N. Chong, Electrochemical oxidation remediation of real wastewater effluents — a review, Process Saf. Environ. Prot., 113 (2018) 48–67.

[5] C.A. Martínez-Huitle, M. Panizza, Electrochemical oxidation of organic pollutants for wastewater treatment, Curr. Opin. Electrochem., 11 (2018) 62–71.

[6] O. Garcia-Rodriguez, E. Mousset, H. Olvera-Vargas, O. Lefebvre, Electrochemical treatment of highly concentrated wastewater: a review of experimental and modeling approaches from lab- to full-scale, Crit. Rev. Env. Sci. Technol., 52 (2020) 240–309.

[7] P. Cañizares, J. García-Gómez, J. Lobato, M.A. Rodrigo, Modeling of wastewater electro-oxidation processes part I. general description and application to inactive electrodes, Ind. Eng. Chem. Res., 43 (2004) 1915–1922.

[8] P. Cañizares, J. García-Gómez, J. Lobato, M.A. Rodrigo, Modeling of wastewater electro-oxidation processes part II. application to active electrodes, Ind. Eng. Chem. Res., 43 (2004) 1923–1931.

[9] A.M. Polcaro, M. Mascia, S. Palmas, A. Vacca, Kinetic study on the removal of organic pollutants by an electrochemical oxidation process, Ind. Eng. Chem. Res., 41 (2002) 2874–2881.

[10] O. Scialdone, A. Galia, S. Randazzo, Electrochemical treatment of aqueous solutions containing one or many organic pollutants at boron doped diamond anodes. Theoretical modeling and experimental data, Chem. Eng. J., 183 (2012) 124–134.

[11] P. Trinidad, C. Ponce de León, F.C. Walsh, The application of flow dispersion models to the FM01-LC laboratory filter-press reactor, Electrochim. Acta, 52 (2006) 604–613.

[12] P. Mavros, Technical note validity and limitations of the closed-vessel analytical solution to the axial dispersion model, Miner. Eng., 5:9 (1992) 1053–1060.

[13] F.F. Rivera, M.R. Cruz-Díaz, E.P. Rivero, I. González, Analysis and interpretation of residence time distribution experimental curves in FM01-LC reactor using axial dispersion and plug dispersion exchange models with closed–closed boundary conditions, Electrochim. Acta, 56 (2010) 361–371.

[14] G. Rodríguez, F.Z. Sierra-Espinosa, J. Teloxa, A. Álvarez, J.A. Hernández, Hydrodynamic design of electrochemical reactors based on computational fluid dynamics, Desal. Water Treat., 57 (2015) 22968–22979.

[15] L. Castañeda, R. Antaño, F.F. Rivera, J.L. Nava, Computational fluid dynamic simulations of single-phase flow in a spacer-filled channel of a filter-press electrolyzer, Int. J. Electrochem. Sci., 12 (2017) 7351–7364.

[16] D.P. Ghumra, C. Agarkoti, P.R. Gogate, Improvements in effluent treatment technologies in common effluent treatment plants (CETPs): review and recent advances, Process Saf. Environ. Prot., 147 (2021) 1018–1051.

[17] J.L. Nava, C. Ponce de León, Reactor Design for Advanced Oxidation Processes, Handbook of Environmental Chemistry, 61, Springer, Singapore, 2018, pp. 263–286.

[18] J. Radjenovic, D.L. Sedlak, Challenges and opportunities for electrochemical processes as next-generation technologies for the treatment of contaminated water, Environ. Sci. Technol., 49 (2015) 11292–11302.

[19] F.C. Moreira, R.A.R. Boaventura, E. Brillas, V.J.P. Vilar, Electrochemical advanced oxidation processes: a review on their application to synthetic and real wastewaters, Appl. Catal., B, 202 (2017) 217–261.

[20] N. Wachter, N. Bocchi, R.C. Rocha-Filho, Use of a turbulence promoter in an electrochemical filter-press reactor: consolidated evidence of significant enhancement of organics mass transport and degradation rates, Sep. Purif. Technol., 276 (2021) 119292, doi: 10.1016/j.seppur.2021.119292.

[21] A. Kapałka, G. Fóti, C. Comninellis, Kinetic modelling of the electrochemical mineralization of organic pollutants for wastewater treatment, J. Appl. Electrochem., 38 (2008) 7–16.

[22] C.A. Martínez-Huitle, L.S. Andrade, Electrocatalysis in wastewater treatment: recent mechanism advances, Quim. Nova, 34 (2011) 850–858.

[23] M. Rueffer, D. Bejan, N.J. Bunce, Graphite: an active or an inactive anode?, Electrochim. Acta, 56 (2011) 2246–2253.

[24] O. Scialdone, Electrochemical oxidation of organic pollutants in water at metal oxide electrodes: a simple theoretical model including direct and indirect oxidation processes at the anodic surface, Electrochim. Acta, 54 (2009) 6140–6147.

[25] C.A. Martínez-Huitle, M.A. Rodrigo, I. Sirés, O. Scialdone, Single and coupled electrochemical processes and reactors for the abatement of organic water pollutants: a critical review, Chem. Rev., 115 (2015) 13362–13407.

[26] T. Zier, S. Bouafia-Chergui, M. Chabani, Anodic oxidation of synthetic refinery effluent on lead anode: mass transport and charge rate balance, Water Sci. Technol., 84 (2021) 2422–2431.

[27] P. Trinidad F.C. Walsh, Hydrodynamic behaviour of the FM01-LC reactor, Electrochim. Acta, 41 (1996) 493–502.

[28] M. Griffiths, C.P. De León, F.C. Walsh, Mass transport in the rectangular channel of a filter-press electrolyzer (the FM01-LC reactor), AlChE J., 51 (2005) 682–687.

[29] I. El Gheriany, M.H. Abdel-Aziz, E.S.Z. El-Ashtoukhy, G.H. Sedahmed, Electrochemical removal of urea from wastewater by anodic oxidation using a new cell design: an

experimental and modeling study, Process Saf. Environ. Prot., 159 (2022) 133–145.
[30] J.A. Yàñez-Varela, V.X. Mendoza-Escamilla, A. Alonzo-Garcia, S.A. Martinez-Delgadillo, I. Gonzalez-Neria, C. Gutiérrez-Torres, CFD and experimental validation of an electrochemical reactor electrode design for Cr(VI) removal, Chem. Eng. J., 349 (2018) 119–128.
[31] J.E. Lira-Teco, F. Rivera, O. Farías-Moguel, J. Torres-González, Y. Reyes, R. Antaño-López, G. Orozco F. Castañeda-Zaldivar, Comparison of experimental and CFD mass transfer coefficient of three commercial turbulence promoters, Fuel, 167 (2016) 337–346.
[32] N.D. Muazu, N. Jarrah, A. Bukhari, Kinetic modeling of electrochemical oxidation of phenol on boron-doped diamond anode in the presence of some inorganic species, Desal. Water Treat., 56 (2015) 3005–3012.
[33] A.N. Ghanim, Perspectives of electrochemical oxidation parameters in PRW treatment, Int. J. Environ. Waste Manage., 26 (2020) 349–361.
[34] K. Scott, J. Lobato, Determination of a mass-transfer coefficient using the limiting-current technique, Chem. Educ., 7 (2022) 214–219.